Predicting Bond Dissociation Energies and Bond Lengths of Coordinatively Unsaturated Vanadium–Ligand Bonds

Junwei Lucas Bao,*[,†,‖] Bradley K. Welch,[§,‖] Inga S. Ulusoy,[§,○] Xin Zhang,[♦,‡] Xuefei Xu,[¶] Angela K. Wilson,*[,§] and Donald G Truhlar*[,‡]

[†]*Department of Chemistry, Boston College, Chestnut Hill, Massachusetts 02467, USA*

[§]*Department of Chemistry, Michigan State University, 578 S Shaw Lane, East Lansing, MI 48824-1322, USA*

[○]*Theoretical Chemistry, Institute of Physical Chemistry, Heidelberg University, Im Neuenheimer Feld 229, 69120 Heidelberg, Germany*

[♦]*State Key Laboratory of Chemical Resource Engineering, Beijing Advanced Innovation Center for Soft Matter Science and Engineering, Beijing University of Chemical Technology, Beijing 100029, People's Republic of China*

[‡]*Department of Chemistry, Chemical Theory Center, Inorganometallic Catalyst Design Center, and Minnesota Supercomputing Institute, University of Minnesota, 207 Pleasant Street SE, Minneapolis, MN 55455-0431, USA*

[¶]*Center for Combustion Energy, Department of Energy and Power Engineering, and Key Laboratory for Thermal Science and Power Engineering of Ministry of Education, Tsinghua University, Beijing 100084, China*

[‖]J.L.B. and B.K.W. contributed equally to this work.

ABSTRACT: Understanding the electronic structure of coordinatively unsaturated transition-metal compounds and predicting their physical properties are of great importance for catalyst design. Bond dissociation energy D_e and bond length r_e are two of the fundamental quantities for which good predictions are important for a successful design strategy. In the present work, recent experimentally measured bond energies and bond lengths of VX diatomic molecules (X = C, N, S) are used as a gauge to consider the utility of a number of electronic structure methods. Single-reference methods are one focus because of their efficiency and utility in practical calculations, and multireference configuration interaction (MRCISD) methods and a composite coupled cluster (CCC) method are a second focus because of their potential high accuracy. The comparison is especially challenging because of the large multireference M diagnostics of these molecules, in the range 0.15–0.19. For the single-reference methods, Kohn-Sham density functional theory (KS-DFT) has been tested with a variety of approximate exchange-correlation functionals. Of these, MOHLYP provides the bond dissociation energies in best agreement with experiments, and BLYP provides the bond lengths that are in best agreement with experiments; but by requiring good performance for both the D_e and r_e of the vanadium compounds, MOHLYP, MN12-L, MGGA_MS1, MGGA_MS0, O3LYP, and M06-L are the most highly recommended functionals. The CCC calculations include up to pentuple-connected excitations for the valence electrons and up to quadruple connected excitations for the core-valence terms; this results in highly accurate dissociation energies and good bond lengths. Averaged over the three molecules, the mean unsigned deviation of CCC bond energies from experimental ones is only 0.4 kcal/mol, demonstrating excellent convergence of theory and experiment.

TOC Graphic

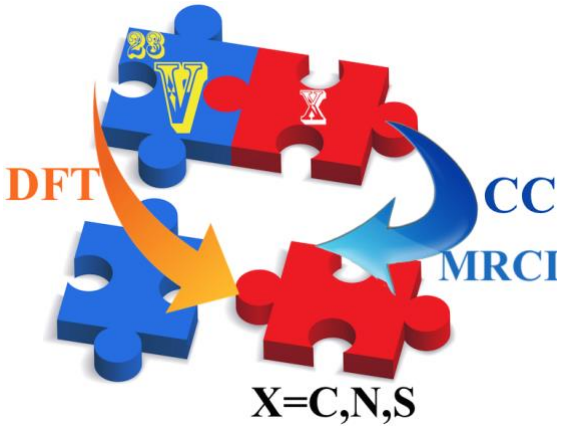

1. Introduction

Computationally guided catalyst design holds great promise for chemistry.[1,2] The most promising catalysts for future development involve coordinatively unsaturated transition metals as the active site. In recent years, Evans–Polanyi-type correlations[3] between the energetics of reaction intermediates and transition barriers have been widely used for catalyst screening.[4-,6] The physical quantities (which may or may not be experimentally measurable) that are used for constructing this kind of correlation relation are called the descriptors[7-,9], and the bond dissociation energy and bond length, being measurable, are descriptors of great interest. Bond dissociation energies of vapor-phase transition-metal-containing molecules are among the most highly sought data, because they provide the prototypes of these bonds and are as free as possible from environmental effects. In the present study, the focus is on the bond dissociation energies and bond lengths of three vanadium–ligand diatomic radicals VX where X = C, N, or S; these molecules are chosen as targets because they have been carefully studied experimentally–with both bond energies[13] and bond distances[16] being available. The experimental uncertainty of the bond energies is not based on statistical analysis, but instead includes estimates of the effects of laser linewidth, calibration error, and a subjective assessment of the sharpness of the observed predissociation threshold. Mores and co-workers provide this in parentheses, in units of the last reported digits: on VC, VN, and VS, these are given as 4.1086(25), 4.9968(20), and 4.5353(25) eV, respectively. Here 4.1086(25) means 4.1086 ± 0.0025 eV. The uncertainty in the experimentally determined rovibrationally averaged bond lengths (r_0) is accurate to the 5th digit.

Vanadium acting as a reactive center can offer versatile catalytic functionalities; recent studies such as catalyzing polymerization reactions,[17] photoinduced water splitting[18], oxidative dehydrogenation of propane,[19] biological mutant reactions,[20] C–H bond activation,[21] and dinitrogen reduction[22] are some examples of applications motivating this work. A recent review covers reactions catalyzed by homogeneous and supported vanadium complexes from 2008 to 2018.[23] Installation of vanadium catalysts on covalent organic frameworks[24] and metal–organic frameworks[25] is expected to open additional possibilities. The current study focuses on the fundamental issue of choosing suitable density functionals for practical catalyst design of catalysts involving vanadium. Benchmark-quality thermochemical data is useful for testing the reliability of predictions for reaction energies and barrier heights by both density functional theory and wave function methods (such as the composite method employed in this work), but such data is rare for polyatomic complexes containing transition metal elements. We therefore

take the opportunity afforded by the accurate bond energies that have become available for diatomic vanadium compounds, which provide an opportunity to test exchange-correlation functionals and high-quality composite wave function methods for their ability to predict accurate vanadium bond energies. We focus on bond energies rather than orbital analysis of bonding because the conclusions about bond energy accuracy are likely to be more transferable to larger systems than conclusions about bonding patterns. With regard to the latter, we emphasize that for transition-metal systems, the correct description of bonding cannot be properly understood by using an easily interpretable single electronic configuration, which means that the analysis of neither density function calculations nor composite methods provide simple pictures of the bonding. This is especially so because the broken-symmetry electronic configuration given by a density functional calculation should not be directly compared to the one given by a multiconfigurational wave function method and because the wave function methods achieve high accuracy only when the concerted effect of many high-order excitations is included. Therefore we focus on bond energies and geometry.

Open-shell transition metal systems provide great challenges for electronic structure methods due to their strongly correlated, inherently multiconfigurational character, and they typically require multi-configurational wave functions (i.e., linear combinations of Slater determinants) approach even for a qualitatively correct zero-order description of their electronic structures. Such multireference methods include the complete-active-space perturbation theory (CASPT2)[26] and the multireference perturbation theory (MRPT2)[27-29] based on the complete-active space self-consistent field (CASSCF)[30] theory. Although these methods can be quite important in the description of the electronic structure, in areas such as practical computational catalysis and organometallic chemistry, the wide application of such methods is typically not ideal, as (a) selection of a well-chosen active is not always intuitive and achieving reliable accuracy in the prediction of properties, at times, can be considered an art form; and (b) the necessary active space is often too large for practical calculations. Although progress is being made in utilizing smaller active spaces and a more systematic approach,[31-33,34] the treatment of large systems is still dominated by calculations employing single-reference methods, i.e., methods with single-configuration reference wave functions. Two major classes of single-reference methods that are often utilized for structural and energetic properties are coupled-cluster theory[35-] with the single and double excitations and a quasiperturbative treatment of connected triple excitations[38] [CCSD(T)] and Kohn-Sham density functional theory[39] (KS-

DFT). Each method has its limitations. Although KS-DFT is quite affordable, it can be unreliable if the exchange-correlation density functional cannot overcome the unphysical nature of a single-configuration reference.[40] Nevertheless, there are cases for which a well-designed density functional can be competitive with CCSD(T) for transition metal systems.[41] Coupled-cluster methods can be highly accurate, providing excellent agreement with experiments,[42,43,44] but they requires very large basis sets for satisfactory accuracy, and for strongly correlated systems, typically, the treatment of high-order excitations (i.e., triple-excitations, quadruple-excitations) is necessary, resulting in a computationally costly approach. A widely used approach to alleviate the cost burden is to use an additive composite thermochemical scheme. Composite schemes attempt to obtain a certain level of accuracy and, rather than do one expensive computation, perform a series of computations to obtain highly accurate energy at a reduced cost.

There have been a number of DFT and coupled-cluster benchmark studies performed on 3d and 4d species, and we will give only a representative selection of references, including applications to metal atoms,[45-48] metal–metal diatomic molecules,[49-51] metal–ligand complexes,[52-61] and metal-centered catalytic reactions,[60-69] demonstrating a broad spectrum of quality, ranging from significant deviation to good agreement with experiment.

In this work, a number of classes of approximate exchange-correlation (XC) density functionals have been considered including generalized gradient approximation (GGA), meta-GGA, non-separable gradient approximation (NGA), meta-NGA, global-hybrid GGA, global-hybrid meta-GGA, range-separated hybrid GGA, range-separated hybrid NGA, range-separated hybrid GGA with molecular mechanics (MM) corrections, and screened-exchange NGA and meta-NGA functionals.

Multi-reference configuration interaction (MRCISD) calculations[70,71] were also carried out to provide a comparison of different effects (i.e., basis set effects, relativistic effects, and multireference character). An advantage of MRCISD calculations is that they are in principle improvable in two ways – by increasing the size of the active space to include the main multireference character with spin-adapted configurations and by raising the excitation level. In a DFT approach, the multireference character of the electronic ground state can, to some extent, be described by using broken-symmetry solutions, often leading to spin contamination to a varying extent.

2. Computational methods

2.1. Density functionals

The exchange-correlation (XC) functionals selected for the current work are tabulated in Table 1 along with references. Basis sets are aug-cc-pwCVTZ-DK[72] for V, aug-cc-pVTZ-DK[73-76] for C and N, and aug-cc-pV(T+d)Z-DK[77-79] for S (i.e., the aug-cc-pV(T+d)Z exponents are used with the DK set's *s* and *p* contraction coefficients). The second-order Douglas-Kroll-Hess (DKH2) Hamiltonian[80,81] is used for describing scalar relativistic effects; we note that this uses a Gaussian nuclear model.[82] Electronic integrals are computed based on a grid of 974 angular points per shell and 99 radial shells. *Gaussian 09*[83] and a locally modified version[84] were used in the KS-DFT calculations.

Table 1. Exchange-correlation (XC) functionals tested in this work

Type	XC functional	X^a	Ref.
GGA	PBEsol	0	85
	SOGGA	0	86
	SOGGA11	0	87
	BLYP	0	88,89
	MOHLYP	0	90
	OLYP	0	91,92
	OreLYP	0	93
	PBE	0	94
	revPBE	0	95
	RPBE	0	96
NGA	GAM	0	97
	N12	0	98
meta-GGA	M06-L	0	99
	revM06-L	0	100
	M11-L	0	101
	MGGA_MS0	0	102
	MGGA_MS1	0	102
	MGGA_MS2	0	102
	τ-HCTH	0	103
meta-NGA	MN12-L	0	104
	MN15-L	0	105
Global-hybrid GGA	B1LYP	25	106
	B3LYP	20	107
	B97-1	21	108
	B97-3	26.93	109
	MPW1B95	31	110
	MPW1K	42.8	111
	MPW3LYP	21.8	112
	MPWB1K	44	110
	O3LYP	11.61	113
	PBE0	25	114
	SOGGA11-X	40.15	115
Global-hybrid meta-GGA	MGGA_MS2h	9	102
	M05	28	116
	M05-2X	56	117,118
	M06	27	119,120
	revM06	40.41	121
	M06-2X	54	117,120
	M06-HF	100	122
	M08-HX	56.79	118
	M08-SO	52.23	118
	PW6B95	28	123
	PWB6K	46	123
	TPSSh	10	124
	τ-HCTHhyb	15	125
Global-hybrid meta-NGA	MN15	44	126
Range-separated hybrid GGA	HSE06	0–25	127,128
	ωB97X	15.77–100	129
Range-separated hybrid GGA + MM[b]	ωB97X-D	22.2–100	130
Range-separated hybrid meta-GGA	M11	42.8–100	131
	revM11	22.5–100	132
Screened-exchange NGA	N12-SX	0−25	133
Screened-exchange meta-NGA	MN12-SX	0−25	133

[a] X is the percentage of nonlocal Hartree–Fock exchange. When a range is given, the first value is for small interelectronic distances, and the second is for large interelectronic distances.

[b] MM denotes the addition of molecular mechanics (also called an empirical dispersion correction), which in this case corresponds to atom-atom pairwise damped dispersion terms added post-SCF to the calculated energy.

2.2. Composite Coupled Cluster (CCC) method

Many *ab initio* composite methods are available.[56,57,134-144] High accuracy composite thermochemistry schemes include treatments of electron correlation beyond CCSD(T). In previous work, we have found out that even for a seemingly simple main-group reaction, it could be vital to include the excitations higher than quadruples for achieving reliable accuracy.[145] A prior beyond-CCSD(T) composite-method study by Cheng et al. applied a variation of the Highly Accuracy Extrapolated *ab initio* Thermochemistry (HEAT) method[141,142,143] to the 3d transition metals with good agreement with experiment.[44] Here, both as a point of comparison and to check the MRCISD approach presented in section 2.5, we use a coupled-cluster (CC) composite scheme that includes higher-order excitations beyond CCSD(T), in a way similar to HEAT and the Feller-Peterson-Dixon (FPD) method. The Composite Coupled Cluster (CCC) method used here is described next.

The Composite Coupled Cluster (CCC) energy is given by

$$E(\mathrm{CCC}) = E\left(\frac{\mathrm{CCSD(T)}}{\mathrm{CBS}}\right)(\mathrm{Core}) + \Delta\mathrm{CCSDT}_{\mathrm{VAL}} + \Delta\mathrm{CCSDTQ}_{\mathrm{VAL}} + \Delta\mathrm{CCSDTQP}_{\mathrm{VAL}} + \Delta_{\mathrm{CV}} + \Delta\mathrm{Rel}_{\mathrm{VAL}} \quad (1)$$

$$\Delta\mathrm{CCSDT}_{\mathrm{VAL}} = E(\mathrm{CCSDT/CBS}) - E[\mathrm{CCSD(T)/CBS}] \quad (2)$$

$$\Delta\mathrm{CCSDTQ}_{\mathrm{VAL}} = E(\mathrm{CCSDTQ/PVTZ}) - E(\mathrm{CCSDT/PVTZ}) \quad (3)$$

$$\Delta\mathrm{CCSDTQP}_{\mathrm{VAL}} = E(\mathrm{CCSDTQP/PVDZ}) - E(\mathrm{CCSDTQ/PVDZ}) \quad (4)$$

$$\Delta_{\mathrm{CV}} = E\left(\frac{\mathrm{CCSDT}}{\mathrm{PWCVTZ}}\right)(\mathrm{Core}) - E\left(\frac{\mathrm{CCSDT}}{\mathrm{PWCVTZ}}\right) + E[\mathrm{CCSDT(Q)/PWCVTZ}](\mathrm{Core}) - E[\mathrm{CCSDT(Q)/PWCVTZ}] \quad (5)$$

$$\Delta\mathrm{Rel}_{\mathrm{VAL}} = E[\mathrm{CCSD(T)|DKH/APVQZDK}] - E[\mathrm{CCSD(T)/APVQZ}] \quad (6)$$

where CCSDT denotes coupled-cluster singles, doubles, and triples, CCSDTQ denotes coupled-cluster singles, doubles, triples, and quadruples, CCSDTQP denotes coupled-cluster singles, doubles, triples, quadruples, and pentuples. Theoretical details of the higher order coupled cluster methods are discussed in ref 146. Note that the valence and core-valence energies are not computed separately at the CCSD(T) level, but they are calculated separately for the higher-order terms. “VAL” stands for valence correlation only, *i.e.*, frozen core, and “Core” stands for core correlation being also included.

The CCSD(T) component E(CCSD(T)/CBS)(Core), was obtained with an ℓ^{-3} CBS extrapolation[147] with aug-cc-pWCVQZ and aug-cc-pWCV5Z basis sets.[72-75,78] Core electrons were also correlated in the total CCSD(T) energy term E(CCSD(T)/CBS)(Core). The reference and coupled cluster energy were not separated. Valence relativistic effects, $\Delta\mathrm{Rel}_{\mathrm{VAL}}$, were included with the second-order DKH integrals with CCSD(T)/aug-cc-pVQZ-DK (*i.e.*, APVQZDK),[76] *i.e.*, CCSD(T)|DKH. (DKH was only applied to the valence electrons at the CCSD(T) level.) This component was calculated by *Molpro 2015.1*.[158]

The ΔCCSDT$_{\mathrm{VAL}}$ component was extrapolated to the complete basis set (CBS) with the cc-pVTZ (*i.e.*, PVTZ) and cc-pVQZ (*i.e.*, PVQZ) basis sets.

The ΔCCSDTQ$_{\mathrm{VAL}}$ contribution was determined with the cc-pVTZ (*i.e.*, PVTZ) basis set.

The ΔCCSDTQP$_{\mathrm{VAL}}$ component was computed with the cc-pVDZ (*i.e.*, PVDZ) basis set.

The Δ_{CV} component was determined with CCSDT(CORE) and CCSDT(Q)(CORE) with the cc-pwCVTZ set in an analogous fashion to eqs 2 and 3. Details of CCSDT(Q) are discussed in ref 148.

All post-CCSD(T) contributions (CCSDT, CCSDTQ, CCSDTQP) to the total energy were obtained with *MRCC*[149]. In eq 2, the CCSD(T) was determined with MRCC and not *Molpro* to maintain consistency between coupled-cluster formulations.

Atomic spin-orbit energies were derived from reference 151 and the molecular spin-orbit energies for VC and VN was obtained from the methods described in section 3.1.

2.3. Multi-reference configuration interaction (MRCISD) calculations

The same basis sets as for the DFT calculations (see section 2.1) are used for the MRCISD calculations, except for VS, where the cc-pVQZ basis set was used because it gave a significant improvement in the results. The DKH Hamiltonian of order two (VC and VS) and order four (VN) was used to describe scalar relativistic effects. The equilibrium dissociation energy D_e is then given by

$$D_e = E(\mathrm{V+X})_{\mathrm{inf}} - E(\mathrm{VX})_{\mathrm{eq}} + E(\mathrm{SO})_{\mathrm{X}} + \mathrm{E(SO)_V} - E(\mathrm{SO})_{\mathrm{VX}} \quad (7)$$

where $E(\mathrm{V+X})_{\mathrm{inf}}$ is the energy of the atoms at a large distance (R = 15 Å), and $E(\mathrm{VX})_{\mathrm{eq}}$ is the energy of the molecule at equilibrium; $E(\mathrm{SO})_{\mathrm{X}}$, and $E(\mathrm{SO})_{\mathrm{V}}$ are the spin-orbit energy of the atoms; $E(\mathrm{SO})_{\mathrm{VX}}$ is the spin-orbit energy of the molecule.

The active space for VC included nine electrons in ten molecular orbitals (MOs), i.e., CAS (9e,10o) was chosen. For VN and VS, we used CAS (10e,10o) and CAS(11e,10o) active spaces,

respectively. All calculations were run with no frozen orbitals in the initial multiconfiguration self-consistent field (MCSCF) calculations. In the MRCISD calculations and for VC and VN, six orbitals were set as core and thus excluded from excitations into virtual orbitals; and four orbitals were set as closed, i.e., they were doubly occupied in the reference space, but they still contribute to the correlation energy through excitations into the virtual orbitals in the external configurations.

The calculations are carried out in C_{2v} point group symmetry, and there are four a_1 orbitals, one b_1 orbital, and one b_2 orbital in the core for both VC and VN. (The a_1, b_1, and b_2 orbitals are classified as σ/σ*, π/π*, π/π*, respectively.) The closed space consists of two a_1, one b_1 a_1, and b_2 orbital. The active space contains five a_1 MOs, two b_1 MOs, two b_2 MOs, and one a_2 MO (which is the metal d orbital). In the default active space, the orbitals defined here as "closed" are part of the core space, but they have been found to be quite significantly correlated and thus moved from the core to the closed space. The largest difference upon dissociation is observed for the metal d orbital, and the high-lying sigma orbitals.

For VS, 14 orbitals were set as core orbitals, and ten were treated as active, resulting in a core space with (8,3,3,0) MOs for (a_1,b_1,b_2,a_2) symmetry, and an active space with (5,2,2,1) MOs for (a_1,b_1,b_2,a_2) symmetry, that can be characterized as (σ/σ*, π/π*, π/π*, metal d).

All MRCISD calculations were performed using the *Molpro 2015.1* package.[158]

3. Computational details

The experimental bond dissociation energy is called D_0, where the subscript denotes dissociation from the zero-point vibrational level.[150] We calculate this as

$$D_0 = D_e - \mathrm{ZPE} \tag{8}$$

where D_e is the equilibrium dissociation energy including SO energies, which is given by

$$D_e = E(\mathrm{V}) + E(\mathrm{X}) - E(\mathrm{VX}) + \Delta E^{SO} \tag{9}$$

with

$$\mathrm{D}E^{SO} = E^{SO}(\mathrm{V}) + E^{SO}(\mathrm{X}) - E^{SO}(\mathrm{VX}, r_e) \tag{10}$$

where E(V), E(X) and E(VX) are the Born-Oppenheimer energies of V, X, and VX (X = C, N, S); and E^{SO}(V), E^{SO}(X), and E^{SO}(VX) are their spin-orbit energies, r_e is the equilibrium internuclear distance, and ZPE is the zero-point vibrational energy. The following subsections explain how each of these terms is calculated. Note that the MRCISD calcuiations are not size

extensive and the active space needs to be preserved and treated equally for the atoms and the diatomic (which is best assured by keeping the total number of orbitals constant in the calculation), so we replace eq 9 for that method by

$$D_e = E(\mathrm{VX})_{\mathrm{inf}} - E(\mathrm{VX}) \qquad (11)$$

where $E(\mathrm{VX})_{\mathrm{inf}}$ is a supermolecule calculation at large V–X distance. We use the same calculation of $\mathrm{D}E^{\mathrm{SO}}$ for all methods tested, but r_e and D_e are calculated for every method tested.

3.1. Spin-orbit (SO) coupling energies

Spin-orbit coupling, which is a vector relativistic effect, is not negligible for open-shell vanadium compounds. The spin-orbit energy is the energy difference of the lowest spin-orbit eigenstate from the multiplet-averaged state; the average values are averaged over all J reported in the database. Spin-orbit energies for vanadium (^{4}F state), carbon (^{3}P state), nitrogen (^{4}S state), and sulfur (^{3}P state) atoms are computed from the NIST database,[151] and their values are –0.9 kcal/mol, –0.1 kcal/mol, 0 kcal/mol, and –0.6 kcal/mol respectively.

Vanadium sulfide (VS) is a linear molecule with a $^4\Sigma^-$ ground state; therefore, its spin-orbit coupling energy is (in the usual first-order approximation) zero by symmetry. For VC ($^2\Delta_{3/2}$ state) and VN ($^3\Delta_1$ state), the spin-orbit matrix elements and eigenstates were computed by the state-averaged CASSCF (SA-CASSCF) method[152,153] averaged over two states using the full Breit-Pauli spin-orbit operator.[154,155] In the CASSCF calculations, the ma-TZVP basis set[156] was used for C and N, and the def2-TZVP basis set[157] was used for V. A full valence active space was used in this work, i.e., the active space was CAS (9e, 10o) for VC and CAS (10e, 10o) for VN, respectively. All spin-orbit computations were performed with *Molpro 2015.1*.[158]

In order to test the approach for estimating the spin-orbit energies of the molecules, we did a test calculation for V atom. With the def2-TZVP basis set, we calculate a spin-orbit energy of –0.926 kcal/mol without scalar relativistic effects and -0.915 kcal/mol with either a 2nd-order or 3rd-order Douglas-Kroll-Hess treatment of scalar relativistic effects; these values agree very well with experiment[151] (–0.913 kcal/mol). This gives confidence that our approach yields the accuracy needed for the present work.

3.2. Equilibrium bond length

The computed equilibrium bond length r_e is obtained by geometry optimization. In all calculations, the experimentally determined[13,14,15,16] spin state is used, i.e., the ground-state spin multiplicities ($2S + 1$) for V, C, N, S, VC, VN, and VS are 4 (quartet), 3 (triplet), 4, 3, 2 (doublet), 3 and 4.

In the DFT optimizations, internal coordinates and "tight" convergence criteria are used in the optimization. The spin component Ms is set equal to S, and the self-consistent-field wave function is optimized to a stable broken-symmetry[159,160,161] solution (by using the "stab=(opt, xqc)" keyword and varying the initial guesses that are generated from different density functionals), in order to find the lowest-energy solution. The resultant broken symmetry solution is not a pure state (that is, a spin eigenstate); the computed $<S^2>$ values are tabulated in Supporting Information. For VN and VS, the spin contamination is not significant, while for VC, it is significant.

For CCC calculations, the optimized equilibrium bond distance (r_e) is obtained by CCSD(T)(FC), where FC denotes "frozen core," with the cc-pVQZ basis set.[72,73,75] The MRCISD equilibrium geometry r_e was located by computing the MRCISD energies over internuclear distance r for a range of values and identification of the minimum with an accuracy of three digits after the decimal point for r_e.

3.3. Equilibrium bond dissociation energy

The equilibrium bond dissociation energy D_e is computed at the equilibrium geometry by eq 8 or 11. Two approaches for computing D_e were utilized: (i) E(VX) is based on *optimized* equilibrium geometries, and the D_e obtained in this way is denoted as D_e^{Opt}; (ii) E(VX) is a single-point energies computed based at *experimental* equilibrium geometries, and the D_e obtained in this way is denoted as D_e^{SP}. It will be shown that the values of D_e^{Opt} and D_e^{SP} are very similar.

3.4. Comparative data: Experimental r_0 to experimental r_e

The experimentally measured bond length is in the ground vibrational–rotational state r_0. The computed bond length is the equilibrium bond length r_e, which, for diatomic molecules, corresponds to the interatomic distance at the bottom of the Born-Oppenheimer potential energy curve. For an anharmonic potential, the ground-state bond length is slightly longer than the

equilibrium bond length r_e. To make an appropriate comparison, we convert the r_0 derived from experiment to r_e.

The equilibrium rotational constant B_e and the rotational constant in the zero-point vibrational state B_0 are related by the following equation:[162]

$$B_e = B_0 + \frac{\alpha_e}{2} \tag{12}$$

where the experimental B_0 is used to derive r_0 by:

$$B_0 = \frac{h^2}{8\pi^2 \mu r_0^2} \tag{13}$$

where h is Plank's constant, and μ is the reduced mass of the diatomic molecule. The rotational-vibrational interaction constant α_e is computed as:[162]

$$\alpha_e = \frac{6\sqrt{x_e \nu_e B_e^3}}{\nu_e} - \frac{6B_e^2}{\nu_e} \tag{14}$$

where ν_e is the harmonic vibrational frequency. If the experimental ν_e is not available (as is the case in the present study), we use the scaled harmonic frequency computed by M06-L (with the same basis set used in this work and with DKH2). The scale factor used here is λ^H, which is designed for reproducing the experimental harmonic frequency; λ^H is determined based on a standard database[163], and its value is 0.9986. Based on the assumption of a Morse potential, the anharmonicity parameter x_e can be computed by using D_e and ν_e as follows:[164]

$$x_e = \frac{h\nu_e}{4D_e} \tag{15}$$

where the experimental equilibrium dissociation energy D_e is obtained by adding the zero-point vibrational energy (ZPE) of the diatomic molecule (which is computed at M06-L level and scaled by $\lambda^{ZPE} = 0.9849$) to experimental ground-state dissociation energy D_0.

The experimental B_e is obtained by solving eq 12 iteratively. The experimental equilibrium bond length r_e is then extracted from B_e using the following equation:

$$r_e = \sqrt{\frac{h^2}{8\pi^2 \mu B_e}} \tag{16}$$

The experimental r_0 for VC, VS, and VN are 1.6167 Å, 2.0526 Å and 1.5666 Å;[13] the obtained equilibrium bond lengths r_e are respectively 1.6129 Å, 2.0501 Å, and 1.5634 Å. The values of $\alpha_e/(2x_eB_e)$ for VC, VS, and VN are 0.63, 0.64 and 0.63, which are consistent with the mean value 0.67±0.06 (which is averaged over 93 diatomic molecules) reported by Pekeris.[162]

4. Multireference diagnostics

In the present work, six multireference diagnostics are considered for assessing the multireference characters of the VX molecules.

The first is the square of the coefficient of the leading configuration state function, i.e., C_0^2.

The second diagnostic is the B_1 diagnostic, which is defined as:[90]

$$B_1 = D_e(\text{BLYP}) - D_e(\text{B1LYP//BLYP}) \quad (17)$$

where D_e(BLYP) is the equilibrium dissociation energy computed by the BLYP functional at the BLYP optimized geometry, and D_e(B1LYP//BLYP) is the bond dissociation energy determined by performing single-point energy calculation with the B1LYP functional at the BLYP optimized geometry. The only difference between the B1LYP and BLYP functionals is that 25% of the density-based exchange functional in BLYP is replaced by the Hartree-Fock exchange in the B1LYP functional. A B_1 diagnostic value larger than 10 kcal/mol for a bond is considered to be an indication of multireference character, although sometimes B_1 can be large because of other factors than multireference character.

A more expensive and very popular diagnostic for multireference character is the T_1 diagnostic,[165] which is based on the Frobenius norm of the t_1 vector of the closed-shell coupled-cluster wave function starting from a restricted Hartree-Fock reference:

$$T_1 = \frac{||t_1||}{N_{\text{elec}}^{1/2}} \quad (18)$$

Although it is widely used, it has been found to have a poor correlation with energy-based diagnostics.[166]

A fourth criterion is the D_1 diagnostic,[167] which is an alternative formulation of T_1, but is more closely related to the value of the largest single-excitation amplitude.

The fifth diagnostic is the percentage of the (T) contribution, i.e., the quasiperturbative connected triples amplitude, to the total atomization energy (%TAE) from coupled-cluster calculations.[140] While the T_1 diagnostic is widely utilized, it has been recommended for inorganic species to use a combination of the three diagnostics with the criteria differing from those used for main-group compounds, with $T_1 \geq 0.05$, $D_1 > 0.15$, and |%TAE| > 10% for 3d transition metal species.[168,169]

The fifth diagnostic is the M diagnostic,[170] which is a direct measure of the size of the leading multireference contributions. It is calculated in the present work – as usual – from the

CASSCF wave functions. The M diagnostic has been used to classify multireference character as small ($M <$ 0.05), modest ($0.05 < M < 0.10$), or large ($0.10 > M$).

5. Results and discussion

5.1. Spin-Orbit Computations

The computed spin-orbit energies for VC ($^2\Delta_{3/2}$ state) and VN ($^3\Delta_1$ state) are -0.42 kcal/mol and -0.47 kcal/mol., respectively. (It is zero by symmetry for VS.) There is no experimental result available for VC, but the experimental spin-orbit energy for VN is -0.43 kcal/mol,[15] confirming the validity of our calculation method. We therefore use these calculated values in eq 10, which then goes into eq 8. (We always use experiment for atomic spin-orbit couplings.)

5.2. Multireference characteristics of VX

Shown in Table 2 are the multireference diagnostics for the molecules.

Table 2. Multireference diagnostics, as defined in Section 4

Molecule	C_0^2 from CASSCF[a]	C_0^2 from MRCISD	B_1 (kcal/mol)	T_1	D_1	%TAE	M from CASSCF
VC	0.840	0.745	33.1	0.110	0.219	23.2	0.191
VN	0.852	0.771	37.4	0.063	0.129	19.4	0.153
VS	0.828	0.769	22.3	0.086	0.180	12.6	0.171
Criteria	< 0.90	---	> 10[b]	> 0.05[c]	> 0.15[c]	> 10[d]	> 0.05, 0.10[e]

[a]Molecular values in this column are from ref 169; all other columns are from the present work. [b]Criterion established in ref 90 [c]Criterion established in ref 169 [d]Criterion established in ref 140 [e]Criterion established in ref 170

Although C_0^2 is widely used, it is depreciated for two reasons. First, it has a significant size dependence so it could be deceptive to compare C_0^2 values from the present work to those for larger vanadium-containing complexes. Second, the value of C_0^2 for a CASSCF calculation does not account for correlation between valence and excited states.[169] This is especially noticeable in table 2 where the CASSCF values are significantly higher than the MRCI values. The M diagnostic should not have either of these two detrimental characteristics.

The computed B_1 diagnostics for VC, VN, and VS are 33.1, 37.4, and 22.3 kcal mol^{-1}, all of which are much greater than the threshold value 10 kcal mol^{-1}, suggesting strong multireference character. Included in the table are the results for other diagnostic measures, all indicating the

very strong multireference character of these species.

5.3. Bond length predicted by various XC functionals, CCSD(T), and MRCISD

Table 3 gives the optimized equilibrium bond lengths and their mean unsigned errors (MUEs) as compared to the experimental r_e; Table S1 (in Supporting Information) gives signed errors and mean signed errors (MSEs).

Based on MUEs, the best five functionals for computing r_e(V-C) are, in order of increasing unsigned error, GAM, MOHLYP, BLYP, RPBE, and M06-L, with the unsigned errors being 0.001, 0.002, 0.0023, 0.0055 and 0.0066 Å, respectively. For the equilibrium bond length of VN, BLYP, MOHLYP, RPBE, revPBE, and MGGA_MS1 are the five best functionals; their unsigned errors are 0.002, 0.007, 0.009, 0.010, and 0.012 Å. For VS, the MPW3LYP, MN12-L, OreLYP, and B3LYP functionals result in equilibrium bond lengths that are almost identical to the experimentally measured one; their unsigned errors are smaller than 0.001 Å. For VC and VN, all 53 density functionals underestimate the equilibrium bond length (!), but for VS there 26 underestimates and 27 overestimates.

The functionals are arranged in order of increasing MUE, and the first 15 functionals are all local; the next 5 are hybrid. The average of the mean unsigned errors for the 53 density functionals in table 3 is 0.026 Å, so any functional doing better than this is above average. The functional with the best overall performance for predicting r_e is BLYP with an MUE of 0.005 Å. The other functionals that have an overall accuracy of 0.010 Å or less are RPBE, M06-L, revPBE, OreLYP, MGGA_MS2, MOHLYP, and MGGA_MS1.

At the MRCISD level, the signed errors of r_e for VC, VN, and VS are -0.0034, -0.0011, and 0.0085 Å. The MRCISD calculations result in the most accurate bond length, in comparing both the mean unsigned (0.004 Å) and the mean signed errors (0.001 Å). The CCSD(T) geometry used for the composite CC scheme did not perform as well as MRCISD. The signed errors of r_e by CCSD(T) are 0.007, -0.001, and 0.019 Å for VC, VN, and VS, respectively. The larger bond-length errors in the CCSD(T) calculations are assumed to result from the single-reference character of CCSD(T).

5.4. Bond dissociation energy predicted by various XC functionals, Composite, and MRCISD

The computed equilibrium bond dissociation energy D_e^{Opt} is shown in Table 4, and D_e^{SP} is

provided in Table S. The signed errors are tabulated in Tables S2 and S3. In Tables 4 and 5, it is shown that, for a given XC functional, the computed D_e^{Opt} and D_e^{SP} are very similar. Twelve functionals give an MUE less than or equal to 5.0 kcal/mol for D_e^{Opt}: in order of increasing MUE, these are MOHLYP, τ-HCTHhyb, O3LYP, MN12-L, M11-L, M05, M11, MGGA_MS1, MGGA_MS0, revM06-L, PBE0, HSE06, and M06-L. Among these functionals, the first three (MOHLYP, τ-HCTHhyb, and O3LYP) have MUEs smaller than 3.0 kcal/mol.

The MRCISD calculations result in an MUE of 3.3 kcal mol^{-1} with the largest error for VC (whose bond energy is underestimated by 5.7 kcal/mol). For VN, a fourth-order DKH Hamiltonian was used as the convergence of the energies with respect to the order of DKH Hamiltonian is slow, and for VS, the triple-zeta basis set proved far too insufficient. It should be noted that the convergence of the energies with increasing basis set size is much slower for the wave-function approaches than for density functional methods, which leads to an additional factor increasing the computational demand of the calculation. However, the MRCISD results provide consistently good accuracy for D_e^{SP} and D_e^{Opt}, and this consistency makes this approach very compelling, despite its higher computational demand and the need for user insight in choosing an active space.

Including a quadruples correction (Pople-type with relaxed reference) in the MRCISD calcuations changes the dissociation energies in kcal/mol to 89.0 (VC), 116.8 (VN), and 105.5 (VS), lowering the MUE from 3.0 to 2.5 kcal mol^{-1}, with this MUE dominated by the error for VC.

The composite CC calculations result in an MUE of only 0.4 kcal mol^{-1}. However, the disadvantage of this composite scheme is the scaling, resulting from the computer time for the higher-order correlation terms. The most expensive portion, the core-valence correlation in CCSDT(Q), took 80% of the total wall clock time of the composite scheme. This limits practical calculations to very little beyond diatomics and possibly some triatomics. Eliminating this expensive step increases the MUE on D_e^{Opt} to 0.6 kcal/mol. Table 5 shows how the mean unsigned error increases when we also remove other terms.

Equations 3 and 4 taken together took 15% of the wall clock time, and both of these steps suffer from unfavorable scaling (~ N^8 and N^{10} respectively, where N is the number of basis functions), providing a significant computational bottleneck attribute to the necessary higher-order correlation. However, the advantage of such composite strategies is that they can generally be used in an almost a black box fashion as compared to multireference methods, which often

require significant insight into active space selection. Composite strategies are also beneficial in that identifying systematic routes to improve the energetic prediction often is clear, whereas, though less costly, this is much less clear for density functional theory. As demonstrated by our composite approach here, the inclusion of higher-order coupled-cluster theory improved the results when compared to the experimental D_e.

It is interesting to consider certain sequences of functionals. From M06-L to M06 to M06-2X and then to M06-HF, as X increases (see Table 1), the overall performance of the M06 family of XC functionals degrades. Including HF exchange is useful for (partially) eliminating self-interaction errors (SIEs) in the density functionals.[171] However, adding high amounts of HF exchange brings in significant static-correlation error, which negatively impacts the performance of strongly correlated systems. Therefore, applying density functionals with high amounts of HF exchange for studying transition metal systems is not recommended (agreeing with our original recommendations and with prior work by Wilson et al.).[54] Functionals such as M08-HX, M05-2X, and M06-HF are not designed for treating strong multireference systems, despite their good performance for treating main group thermochemistry and kinetics. However, for computing barrier heights and thermal energetics of transition-metal containing systems, the functional does need some amount of HF exchange for improving the barrier height; in such cases, functionals such as MN15 and M06 should be considered. The present investigation provides a quantitative measure of how much the performance is impacted for bond distance and bond energies by using high X.

Table 6 gives the ranks of various density functionals, composite CC, and MRCISD results based on their MUEs for predicting equilibrium bond dissociation energies and equilibrium bond lengths are shown; a lower rank is better (i.e., rank 1 is best). An average rank is determined with respect to the overall performance, i.e., by averaging the ranks in the three categories. By the measure used in Table 6, MOHLYP, MN12-L, MGGA_MS1, M06-L, and O3LYP are the top five performers among the XC functionals for treating vanadium–ligand bonds. Composite CC (with pentuple excitations) and MRCISD have better overall performance than KS-DFT.

We have shown that all three molecules have high multi-reference character, and the high accuracy of the experimental results in this case makes this a prime and somewhat rare case test of diverse theoretical methods against accurate data for both bond lengths and bond energies of very strongly correlated transition metal compounds.

6. Concluding remarks

Insight about methodological requirements for the prediction of bond dissociation energy and bond length of transition metal compounds with open d-subshells is important to the future of computational catalyst design. Here, a series of calculations by KS-DFT, MRCISD, and a composite coupled-cluster thermochemical scheme have been used to predict bond dissociation energies and bond lengths for three VX molecules with high multireference character and with accurate experimental data available for testing theory. Of the density functional approaches, MOHLYP provides the bond dissociation energies in the best agreement with the experiment, and BLYP gives the bond lengths that are in the best agreement with the experiment. For predictions of both D_e and r_e of these vanadium compounds, MOHLYP, MN12-L, MGGA_MS1, M06-L, and O3LYP are the most highly recommended functionals when a DFT method is to be used for these or similar compounds. Among the theoretical results, MRCISD yields the most accurate bond lengths. The composite CC approach with up to pentuple excitations provides the most accurate bond dissociation energy of the theoretical methods studied here; the use of higher-order coupled-cluster theory in the composite scheme was instrumental in the description of D_e. Three of the density functionals give more accurate bond energies than MRCISD; nevertheless the composite CC and MRCISD results are reasonably consistent, and – given the high level of the composite CC approach – we can say the good agreement (0.4 kcal/mol) of the composite CC results with experiment is quite satisfactory from the point of view of both theory and experiment.

ASSOCIATED CONTENT

Supporting Information.

This material is available free of charge via the Internet at http://pubs.acs.org.

Signed errors, $\langle S^2 \rangle$ values of DFT calculations, D_e^{SP} errors, sample input files. (PDF)

AUTHOR INFORMATION

Corresponding Authors

*J.L.B.: E-mail: lucas.bao@bc.edu

*A.K.W.: E-mail: akwilson@msu.edu

*D.G.T.: E-mail: truhlar@umn.edu

ORCID

Junwei Lucas Bao: 0000-0002-4967-663X

Angela K. Wilson: 0000-0001-9500-1628

Donald G. Truhlar: 0000-0002-7742-7294

Author Contributions

‖J.L.B. and B.K.W. contributed equally to this work.

Notes

The authors declare no competing financial interest.

ACKNOWLEDGMENT

The Wilson group is thanked for useful engagement and discussion in this effort as well as comments on the manuscript. J.L.B. acknowledges the financial support provided by Boston College start-up funding. A.K.W. was supported in part by the National Science Foundation under grant no. CHE-1900086. D.G.T. was supported in part by the U.S. Department of Energy, Office of Basic Energy Sciences, Division of Chemical Sciences, under award DE-SC0012702 (Inorganometallic Catalyst Design Center).

Table 3. Equilibrium bond length r_e (in Å) computed by various electronic-structure methods.

		VC	VN	VS	MUE [a]
Wave function methods	MRCISD	1.610	1.562	2.059	0.004
	CCSD(T)	1.620	1.562	2.069	0.009
Density functionals	BLYP	1.610	1.561	2.060	0.005
	RPBE	1.608	1.555	2.056	0.007
	revPBE	1.604	1.553	2.053	0.008
	M06-L	1.607	1.547	2.052	0.008
	OreLYP	1.600	1.548	2.049	0.010
	MGGA_MS2	1.604	1.550	2.057	0.010
	MOHLYP	1.611	1.557	2.072	0.010
	MGGA_MS1	1.604	1.551	2.060	0.010
	MGGA_MS0	1.603	1.550	2.060	0.011
	GAM	1.612	1.536	2.054	0.011
	MN15-L	1.602	1.542	2.053	0.012
	MN12-L	1.603	1.538	2.051	0.012
	OLYP	1.597	1.545	2.048	0.012
	PBE	1.596	1.549	2.044	0.012
	τ-HCTH	1.596	1.539	2.047	0.015
	MGGA_MS2h	1.596	1.541	2.057	0.015
	TPSSh	1.588	1.541	2.046	0.017
	MN12-SX	1.598	1.531	2.055	0.018
	B3LYP	1.585	1.535	2.051	0.019
	MPW3LYP	1.587	1.533	2.051	0.019
	revM06-L	1.592	1.531	2.057	0.020
	SOGGA11-X	1.570	1.546	2.052	0.021
	O3LYP	1.584	1.530	2.044	0.023
	B97-1	1.583	1.530	2.056	0.023
	PBEsol	1.585	1.540	2.029	0.024
	B1LYP	1.589	1.519	2.055	0.024
	SOGGA	1.584	1.538	2.027	0.026
	HSE06	1.578	1.525	2.041	0.027
	B97-3	1.580	1.522	2.059	0.028
	MPW1K	1.578	1.516	2.045	0.029
	PBE0	1.575	1.524	2.040	0.029
	revM06	1.576	1.512	2.051	0.030
	M06-2X	1.595	1.500	2.059	0.030
	M08-SO	1.577	1.514	2.044	0.031
	M06	1.570	1.522	2.042	0.031
	N12	1.578	1.533	2.023	0.031
	τ-HCTHhyb	1.553	1.530	2.049	0.032
	MPWB1K	1.578	1.508	2.039	0.034
	MPW1B95	1.566	1.517	2.059	0.034
	ωB97X-D	1.532	1.542	2.045	0.036
	N12-SX	1.562	1.521	2.036	0.036
	SOGGA11	1.544	1.532	2.059	0.036
	M11-L	1.572	1.509	2.033	0.038
	M05	1.558	1.511	2.044	0.038
	PW6B95	1.570	1.500	2.040	0.039
	M08-HX	1.566	1.506	2.066	0.040
	ωB97X	1.524	1.535	2.040	0.043
	MN15	1.547	1.514	2.016	0.050
	PWB6K	1.510	1.511	2.044	0.054
	M11	1.513	1.499	2.047	0.056
	M05-2X	1.524	1.499	2.072	0.059
	revM11	1.528	1.497	2.022	0.060
	M06-HF	1.499	1.478	2.081	0.077
	Exptl.[13]	1.613	1.563	2.050	–

[a]MUE is mean unsigned error (average of the absolute errors).

Table 4. D_e^{Opt} (in kcal/mol) computed by various electronic-structure methods.

		VC	VN	VS	MUE [a]
Wave function methods	Composite CC	95.7	116.6	104.8	0.4
	MRCISD	90.5	118.3	102.7	3.0
Density functionals	MOHLYP	97.1	114.5	103.1	1.8
	τ-HCTHhyb	98.7	113.9	106.3	2.1
	O3LYP	98.8	116.9	109.1	2.2
	MN12-L	94.2	108.3	106.0	3.7
	M11-L	97.5	111.0	109.2	3.7
	M05	95.6	107.9	103.2	3.8
	M11	101.8	117.3	111.1	4.0
	MGGA_MS1	91.2	121.1	108.9	4.3
	MGGA_MS0	89.4	120.3	108.2	4.4
	revM06-L	101.9	121.3	108.6	4.5
	PBE0	89.9	111.0	107.4	4.7
	HSE06	89.1	111.0	107.3	4.9
	M06-L	102.0	114.4	112.1	5.0
	MGGA_MS2	92.4	124.1	110.0	5.2
	N12-SX	94.1	105.4	102.9	5.3
	B97-1	90.2	109.7	101.6	5.6
	B3LYP	87.2	112.6	101.5	5.7
	MN15-L	88.5	110.5	108.8	5.8
	MGGA_MS2h	82.8	112.6	103.8	6.3
	TPSSh	100.4	122.1	114.9	6.4
	MN15	89.6	108.5	109.7	6.4
	PW6B95	86.1	106.6	103.6	7.3
	MPW3LYP	85.2	110.5	100.2	7.4
	MPW1B95	85.0	104.7	104.1	8.2
	revM11	84.7	108.3	100.8	8.2
	M06	87.7	102.9	102.2	8.5
	τ-HCTH	112.5	121.9	113.1	9.8
	ωB97X-D	84.2	103.5	98.4	10.7
	GAM	85.9	102.4	115.7	11.7
	B97-3	81.5	102.6	98.7	11.8
	OreLYP	110.1	128.0	115.7	11.9
	OLYP	110.8	130.4	116.5	13.1
	revM06	78.2	95.2	101.9	14.3
	B1LYP	76.8	101.6	94.1	15.3
	BLYP	109.8	138.8	116.4	15.6
	ωB97X	81.2	98.0	92.1	15.7
	RPBE	112.6	136.8	120.3	17.1
	MN12-SX	84.3	88.9	90.9	18.1
	revPBE	114.2	138.4	122.1	18.8
	N12	123.1	123.6	133.6	20.7
	M08-SO	71.3	88.8	96.0	20.7
	M08-HX	72.2	88.9	93.3	21.3
	MPW1K	71.6	84.7	93.2	22.9
	MPWB1K	69.0	86.3	94.1	23.0
	PBE	121.2	146.5	128.2	25.9
	M06-2X	66.3	85.4	88.3	26.1
	M05-2X	67.8	81.4	87.5	27.2
	SOGGA11-X	65.8	76.7	86.7	29.7
	SOGGA11	121.7	147.3	141.1	30.6
	PWB6K	51.5	78.1	91.0	32.6
	PBEsol	131.0	155.4	138.2	35.5
	SOGGA	132.3	155.9	139.9	36.6
	M06-HF	43.4	64.8	75.6	44.8
	Exptl.[13]	96.1	116.7	105.4	–

[a]Mean unsigned errors (MUE): the average of the absolute errors

Table 5. Mean unsigned error in D_e^{Opt} (kcal/mol) for the composite CC method and for the method after each step is subsequently removed from the composite, illustrating the impact of the terms.

Term removed	MUE in D_e^{Opt}
none	0.4
remove CCSDT(Q) term in Δ_{CV}	0.6
also remove CCSDT term in Δ_{CV}	1.6
also remove ΔCCSDTQP	1.9
also remove ΔCCSDTQ	4.0
also remove ΔCCSDT	3.1

Table 6. Rankings for r_e, D_e^{Opt}, D_e^{SP} and the average rank of electronic-structure methods.[a]

	Rank-1[b]	Rank-2[c]	Rank-3[d]	Average rank[e]
Composite CC	6	1	1	1
MRCISD	1	5	5	2
MOHLYP	9	2	2	3
MN12-L	14	6	7	4
MGGA_MS1	10	10	9	5
MGGA_MS0	11	11	10	6
O3LYP	25	4	3	7
M06-L	5	15	13	8
MGGA_MS2	8	16	15	9
τ-HCTHhyb	39	3	4	10
revM06-L	23	12	11	11
MN15-L	13	20	16	12
B3LYP	21	19	19	13
PBE0	33	13	14	14
M11-L	45	7	8	15
MGGA_MS2h	18	21	22	16
HSE06	30	14	17	17
TPSSh	19	22	21	18
B97-1	26	18	18	19
M05	46	8	12	20
M11	52	9	6	21
OreLYP	7	33	31	22
MPW3LYP	22	25	24	23
τ-HCTH	17	29	28	24
GAM	12	31	32	25
BLYP	2	37	37	26
N12-SX	43	17	20	27
RPBE	3	39	39	28
OLYP	15	34	34	29
revPBE	4	41	41	30
M06	37	28	27	31
MPW1B95	41	26	26	32
B97-3	31	32	33	33
PW6B95	47	24	25	34
MN15	50	23	23	35
MN12-SX	20	40	40	36
B1LYP	28	36	36	37

ωB97X-D	42	30	30	38
revM06	34	35	35	39
PBE	16	47	47	40
revM11	54	27	29	41
MPW1K	32	45	44	42
M08-SO	36	43	43	43
N12	38	42	42	44
SOGGA11-X	24	50	50	45
ωB97X	49	38	38	46
M06-2X	35	48	48	47
MPWB1K	40	46	46	48
PBEsol	27	53	53	49
SOGGA	29	54	54	50
M08-HX	48	44	45	51
SOGGA11	44	51	52	52
PWB6K	51	52	49	53
M05-2X	53	49	51	54
M06-HF	55	55	55	55

[a]Ranks are based on the order of the MUEs (mean unsigned errors) for VC, VN and VS, with smaller MUE having higher rank. [b]Rank for bond length r_e. [c]Rank for bond dissociation energy D_e^{Opt}. [d]Rank for bond dissociation energy D_e^{SP}. [e]Average rank is (Rank-1 + Rank-2 + Rank-3)/3.

References

1 Nørskov, J. K.; Bligaard, T.; Rossmeisl, J.; Christensen, C. H. Towards the computational design of solid catalysts. *Nat. Chem.* **2009**, *1*, 37–46.

2 Odoh, S. O.; Cramer, C. J.; Truhlar, D. G.; Gagliardi, L. Quantum-chemical characterization of the properties and reactivities of metal–organic frameworks. *Chem. Rev.* **2015**, *115*, 6051–6111.

3 van Santen, R. A.; Neurock, M.; Shetty, S. G. Reactivity theory of transition-metal surfaces: A Brønsted−Evans−Polanyi linear activation energy−free-energy analysis. *Chem. Rev*. **2010**, *110*, 2005–2048.

4 Medford, A. J.; Vojvodic, A.; Hummelshøj, J. S.; Voss, J.; Abild Pedersen, F.; Studt, F.; Bligaard, T.; Nilsson, A.; Nørskov, J. K. From the Sabatier principle to a predictive theory of transition-metal heterogeneous catalysis. *J. Catal*. **2015**, *328*, 36–42.

5 Abild-Pedersen, F.; Greeley, J.; Studt, F.; Rossmeisl, J.; Munter, T.; Moses, P.; Skulason, E.; Bligaard, T.; Nørskov, J. K. Scaling properties of adsorption energies for hydrogen-containing molecules on transition-metal surfaces. *Phys. Rev. Lett*. **2007**, *99*, 016105-1–016105-4.

6 Michaelides, A.; Liu, Z. P.; Zhang, C. J.; Alavi, A.; King, D. A.; Hu, P. Identification of general linear relationships between activation energies and enthalpy changes for dissociation reactions at surfaces. *J. Am. Chem. Soc*. **2003**, *125*, 3704–3705.

7 Medford, A. J.; Shi, C.; Hoffmann, M. J.; Lausche, A. C.; Fitzgibbon, S. R.; Bligaard, T.; Norskov, J. K. CatMAP: A software package for descriptor-based microkinetic mapping of catalytic trends. *Catal. Lett*. **2015**, *145*, 794–807.

8 Norskov, J. K.; Abild-Pedersen, F.; Studt, F.; Bligaard, T. Density functional theory in surface chemistry and catalysis. *Proc. Natl. Acad. Sci. U. S. A*. **2011**, *108*, 937-943.

9 Li, L.; Sholl, D. S. Computational identification of descriptors for selectivity in syngas reactions on a Mo_2C catalyst. *ACS Catal*. **2015**, *5*, 5174–5185.

10 Simard, B.; Mitchell, S. A.; Rayner, D. M.; Yang, D. S. Structures, Energetics, and Reactivity of Metal Clusters and Metal-Ligand Species in the Gas Phase. In *Metal-Ligand Interactions in Chemistry, Physics and Biology*; Russo N., Salahub D.R., Eds.; NATO Science Series C: Mathematical and Physical Sciences, vol 546; Springer: Dordrecht, 2000; pp. 239-294.

11 Armentrout, P. B. Guided ion beam studies of transition metal-ligand thermochemistry. *Int. J. Mass Spectrom.* **2003***, 227*, 289-302.

12 Morse, M. D. Predissociation measurements of bond dissociation energies. *Acc. Chem. Res.* **2019***, 52*, 119-126.

13 Johnson, E. L.; Davis, Q. C.; Morse, M. D. Predissociation measurements of bond dissociation energies: VC, VN, and VS. *J. Chem. Phys*. **2016**, *144*, 234306.

14 Krechkivska, O.; Morse, M. D. Electronic spectroscopy of diatomic VC. *J. Phys. Chem. A* **2013**, *117*, 13284-13291.

15 Balfour, W. J.; Merer, A. J.; Niki, H.; Simard, B.; Hackettet, P. A. Rotational, fine, and hyperfine analyses of the (0,0) band of the D $^3\Pi$–X $^3\Delta$ system of vanadium mononitride. *J. Chem. Phys*. **1993**, *99*, 3288-3303.

16 Ran, Q.; Tam, W. S.; Cheung, A. C.; Merer, A. J. Laser spectroscopy of VS: Hyperfine and rotational structure of the C $^4\Sigma^-$–X $^4\Sigma^-$ transition. *J. Mol. Spectrosc*. **2003**, *220*, 87-106.

17 Hou, X.; Nomura, K. (Arylimido)vanadium(V)–Alkylidene complexes containing fluorinated aryloxo and alkoxo ligands for fast living ring-opening metathesis polymerization (ROMP) and highly cis-specific ROMP. *J. Am. Chem. Soc*. **2015**, *137*, 4662–4665.

18 Santoni, M.-P.; La Ganga, G.; Mollica Nardo, V.; Natali, M.; Puntoriero, F.; Scandola, F.; Campagna, S. The use of a Vanadium species as a catalyst in photoinduced water oxidation. *J. Am. Chem. Soc.* **2014**, *136*, 8189–8192.

19 Rozanska, X.; Fortrie, R.; Sauer, J. Size-dependent catalytic activity of supported Vanadium oxide species: Oxidative dehydrogenation of propane. *J. Am. Chem. Soc*. **2014**, *136*, 7751–7761.

20 Gupta, R.; Hou, G.; Renirie, R.; Wever, R.; Polenova, T. ^{51}V NMR Crystallography of Vanadium chloroperoxidase and its directed evolution P395D/L241V/T343A mutant: Protonation environments of the active site. *J. Am. Chem. Soc*. **2015**, *137*, 5618–5628.

21 Verma, S.; Nasir Baig, R. B.; Nadagouda, M. N.; Varma, R. S. Photocatalytic C-H activation of hydrocarbons over VO@g-C3N4. *ACS Sus. Chem. Eng.* **2016**, *4*, 2333-2336.

22 Sekiguchi, Y.; Arashiba, K.; Tanaka, H.; Eizawa, A.; Nakajima, K.; Yoshizawa, K.; Nishibayashi, Y. Catalytic reduction of molecular dinitrogen to ammonia and hydrazine using vanadium complexes. *Angew. Chem. Int. Ed.* **2018**, *57*, 9064-9068.

23 Langeslay, R. R.; Kaphan, D. M.; Marshall, C. L.; Stair, P. C.; Sattelberger, A. P.; Delferro, M. Catalytic applications of vanadium: A mechanistic perspective. *Chem. Rev.* **2019**, *119*, 2128-2191.

24 Vardhan, H.; Verma, G.; Ramani, S.; Nafady, A.; Al-Enizi, A. M.; Pan, Y.; Yang, Z.; Yang, H.; Ma, S. Covalent organic framework decorated with vanadium as a new platform for prins reaction and sulfide oxidation. *ACS Appl. Mater. Interfaces* **2019**, *11*, 3070-3079.

25 Wang, X.; Zhang, X.; Li, P.; Otake, K.-i.; Cui, Y.; Lyu, J.; Krzyaniak, M, D.; Zhang, Y.; Li, Z.; Liu, J.; Buru, C. T.; Islamoglu, T.; Wasielewski, M. R.; Li, Z.; Farha, O. K. Vanadium catalyst on isostructural transition metal, lanthanide, and actinide based metal-organic frameworks for alcohol oxidation. *J. Am. Chem. Soc*. **2020**, *141*, 8306-8314.

26 Andersson, K.; Malmqvist, P. Å.; Roos, B. O.; Sadlej, A. J.; Wolinski, K. Second-order perturbation theory with a CASSCF reference function. *J. Phys. Chem*. **1990**, *94*, 5483–5488.

27 Hirao, K. Multireference Møller-Plesset method. *Chem. Phys. Lett*. **1992**, *190*, 374–380.

28 Hirao, K. Multireference Møller-Plesset perturbation theory for high-spin open-shell systems. *Chem. Phys. Lett*. **1992**, *196*, 397–403.

29 Hirao, K. Multireference Møller-Plesset perturbation treatment of potential energy curve of N_2. *Int. J. Quantum Chem*. **1992**, *S26*, 517.

30 Roos, B. O.; Taylor, P. R.; Siegbahn, P. E. M. A complete active space SCF method (CASSCF) using a density matrix formulated super-CI approach. *Chem. Phys*. **1980**, *48*, 157–173.

31 Vogiatzis, K. D.; Li Manni, G.; Stoneburner, S. J.; Ma, D.; Gagliardi, L. Systematic expansion of active spaces beyond the CASSCF limit: A GASSCF/SplitGAS benchmark study. *J. Chem. Theory Comput.* **2015***, 11*, 3010–3021.

32 Odoh, S. O.; Manni, G. L.; Carlson, R. K.; Truhlar, D. G.; Gagliardi, L. Separated-pair approximation and separated-pair pair-density functional theory. *Chem. Sci.* **2016***, 7*, 2399–2413.

33 Bao, J. L.; Sand, A.; Gagliardi, L.; Truhlar, D. G. Correlated-participating-orbitals pair-density functional method and application to multiplet energy splittings of main-group divalent radicals. *J. Chem. Theory Comput.* **2016**, *12*, 4274–4283.

34 Bao, J. L.; Odoh, S. O.; Gagliardi, L.; Truhlar, D. G. Predicting bond dissociation energies of transition-metal compounds by multiconfiguration pair-density functional theory and second-order perturbation theory based on correlated participating orbitals and separated pairs. *J. Chem. Theory Comput.* **2017**, *13*, 616–626.

35 Čížek, J. On the correlation problem in atomic and molecular systems. Calculation of wavefunction components in Ursell-type expansion using quantum-field theoretical methods. *J. Chem. Phys*. **1966**, *45*, 4256–4266.

36 Pople, J. A.; Krishnan, R.; Schlegel, H. B.; Binkley, J. S. Electron correlation theories and their application to the study of simple reaction potential surfaces. *Int. J. Quantum Chem.***1978**, *14*, 545–560.

37 Bartlett, R. J.; Purvis, G. D. Many-body perturbation theory, coupled-pair many-electron theory, and the importance of quadruple excitations for the correlation problem. *Int. J. Quantum Chem*. **1978**, *14*, 561–581.

38 Raghavachari, K.; Trucks, G. W.; Pople, J. A.; Head-Gordon, M. A fifth-order perturbation comparison of electron correlation theories. *Chem. Phys. Lett*. **1989**, *157*, 479–483.

39 Kohn, W.; Sham, L. J. Self-consistent equations including exchange and correlation effects. *Phys. Rev*. **1965**, *140*, A1133–1138.

40 Verma, P.; Truhlar, D. G. Status and challenges of density functional theory. *Trends Chem.* **2020**, *2*, 302–318.

41 Xu, X.; Zhang, W.; Tang, M.; Truhlar, D. G. Do practical standard coupled cluster calculations agree better than Kohn–Sham calculations with currently available functionals when compared to the best available experimental data for dissociation energies of bonds to 3*d* transition metals? *J. Chem. Theory Comput*. **2015**, *11*, 2036–2052.

42 Aoto, Y. A.; De Lima Batista, A. P.; Köhn, A.; De Oliveira-Filho, A. G. S. How to arrive at accurate benchmark values for transition metal compounds: Computation or experiment? *J. Chem. Theory Comput.* **2017**, *13*, 5291–5316.

43 Fang, Z.; Vasiliu, M.; Peterson, K. A.; Dixon, D. A. Prediction of bond dissociation energies/heats of formation for diatomic transition metal compounds: CCSD(T) works. *J. Chem. Theory Comput.* **2017**, *13*, 1057–1066.

44 Cheng, L.; Gauss, J.; Ruscic, B.; Armentrout, P. B.; Stanton, J. F. Bond dissociation energies for diatomic molecules containing 3*d* transition metals: Benchmark scalar-relativistic coupled-cluster calculations for 20 molecules. *J. Chem. Theory Comput.* **2017**, *13*, 1044–1056.

45 Luo, S.; Averkiev, B.; Yang, K. R.; Xu, X.; Truhlar, D. G. Density functional theory of open-shell systems. The 3*d*-series transition-metal atoms and their cations. *J. Chem. Theory Comput*. **2014**, *10*, 102–121.

46 Luo, S.; Truhlar, D. G. How evenly can approximate density functionals treat the different multiplicities and ionization states of 4*d* transition metal atoms? *J. Chem. Theory Comput*. **2012**, *8*, 4112–4126.

47 Schultz, N. E., Zhao, Y.; Truhlar, D. G. Benchmarking approximate density functional theory for *s*/*d* excitation energies in 3*d* transition metal cations. *J. Comput. Chem.* **2007**, *29*, 185–189.

48 Peterson, C.; Penchoff, D. A.; Wilson, A. K. Ab initio approaches for the determination of heavy element energetics: Ionization energies of trivalent lanthanides (Ln = La-Eu). *J. Chem. Phys*. **2015**, *143*, 194109-1–194109-7.

49 Xu, X.; Truhlar, D. G. Performance of effective core potentials for density functional calculations on 3*d* transition metals. *J. Chem. Theory Comput*. **2012**, *8*, 80–90.

50 Zhang, W.; Truhlar, D. G.; Tang, M. Explanation of the source of very large errors in many exchange–correlation functionals for Vanadium dimer. *J. Chem. Theory Comput*. **2014**, *10*, 2399–2409.

51 Schultz, N. E.; Zhao, Y.; Truhlar, D. G. Databases for transition element bonding: Metal−metal bond energies and bond lengths and their use to test hybrid, hybrid meta, and

meta density functionals and generalized gradient approximations. *J. Phys. Chem. A* **2005**, *109*, 4388–4403.

52 Zhao, Y.; Truhlar, D. G. Comparative assessment of density functional methods for 3*d* transition-metal chemistry. *J. Chem. Phys*. **2006**, *124*, 224105-1–224105-6.

53 Li, R.; Peverati, R.; Isegawa, M.; Truhlar, D. G. Assessment and validation of density functional approximations for iron carbide and iron carbide cation. *J. Phys. Chem. A* **2013**, *117*, 169–173.

54 Tekarli, S. M.; Drummond, M. L.; Williams, T. G.; Cundari, T. R.; Wilson, A. K. Performance of density functional theory for 3*d* transition metal-containing complexes: Utilization of the correlation consistent basis sets. *J. Phys. Chem. A* **2009**, *113*, 8607–8614.

55 Laury, M.; DeYonker, N. K.; Jiang, W.; Wilson, A. K. A pseudopotential-based composite method: The relativistic pseudopotential correlation consistent composite approach for molecules containing 4*d* transition metals (Y–Cd) *J. Chem. Phys* **2011**, *135*, 214103-1–214103-10.

56 Jiang, Y.; DeYonker, N.; Determan, J.; Wilson, A. K. Toward accurate theoretical thermochemistry of first row transition metal complexes. *J. Phys. Chem. A.* **2012**, *116*, 870–885.

57 Manivasagam, S.; Laury, M. L.; Wilson, A. K. Pseudopotential-based correlation consistent composite approach (rp-ccCA) for first- and second-row transition metal thermochemistry. *J. Phys. Chem. A*. **2015,** *119*, 6867–6874.

58 Determan, J.; Poole, K; Scalmant, G.; Frisch, M. J.; Janesko, B. G.; Wilson, A. K. Comparative study of nonhybrid density functional approximations for the prediction of 3*d* transition metal thermochemistry. *J. Chem. Theory Comput.* **2017**, *13*, 4907–4913.

59 Lianrui H.; Kejuan C.; Hui C. Modeling σ-Bond activations by Nickel(0) beyond common approximations: How accurately can we describe closed-shell oxidative addition reactions mediated by low-valent late 3*d* transition metal? *J. Chem. Theory Comput.* **2017,** *13*, 4841–4853.

60 Mallah, J.; Ataya, M.; Hasanayn, F. Dimerization of aldehydes into esters by an octahedral d^6-rhodium cis-dihydride catalyst: Inner- versus outer-sphere mechanisms. *Organometallics* **2020,** *39* , 286–294.

61 Minenkov, Y.; Sharapa, D. I; Cavallo, L. Application of semiempirical methods to transition metal complexes: Fast results but hard-to-predict accuracy. *J. Chem. Theory. Comput.* **2018**, *14*, 3428–3439.

62 Bao, J. L.; Yu, H. S.; Duanmu, K.; Makeev, M. A.; Xu, X.; Truhlar, D. G. Density functional theory of the water splitting reaction on Fe(0): Comparison of local and nonlocal correlation functionals. *ACS Catal.* **2015**, *5*, 2070–2080.

63 Weymuth, T.; Couzijn, E. P. A.; Chen, P.; Reiher, M. New benchmark set of transition-metal coordination reactions for the assessment of density functionals. *J. Chem. Theory Comput.* **2014**, *10*, 3092–3103.

64 Hu, L.; Chen, H. Assessment of DFT methods for computing activation energies of Mo/W-mediated reactions. *J. Chem. Theory Comput.* **2015**, *11*, 4601–4614.

65 Sun, Y.; Chen, H. Performance of density functionals for activation energies of Re-catalyzed organic reactions. *J. Chem. Theory Comput*. **2014**, *10*, 579–588.

66 Sun, Y.; Chen, H. Performance of density functionals for activation energies of Zr-mediated reactions. *J. Chem. Theory Comput.* **2013**, *9*, 4735–4743.

67 Minenkov, Y.; Chermak, E.; Cavallo, L. Troubles in the systematic prediction of transition metal thermochemistry with contemporary out-of-the-box methods. *J. Chem. Theory Comput.*

2016, *12*, 1542–1560.

68 Averkiev, B. B.; Zhao, Y.; Truhlar, D. G. Binding energy of d^{10} transition metals to alkenes by wave function theory and density functional theory. *J. Mol. Catal. A: Chem*. **2010**, *324*, 80–88.

69 Yang, L.; Zhang, Q.; Gao, J. Why can normal palladium catalysts efficiently mediate aerobic C–H hydroxylation of arylpyridines by intercepting aldehyde autoxidation? A nascent palladium(III)–peracid intermediate makes a difference. *Inorg. Chem.* **2019**, *58*, 4376–4384.

70 Knowles, P. J.; Werner, H.-J. An efficient method for the evaluation of coupling coefficients in configuration interaction calculations. *Chem. Phys. Lett.* **1988**, *145*, 514–522.

71 Werner, H.-J.; Knowles, P. J. An efficient internally contracted multiconfiguration-reference configuration interaction method. *J. Chem. Phys*. **1988**, *89*, 5803–5814.

72 Balabanov, N. B.; Peterson, K. A. Systematically convergent basis sets for transition metals. I. All-electron correlation consistent basis sets for the 3*d* elements Sc–Zn. *J. Chem. Phys*. **2005**, *123*, 064107-1–064107-15.

73 Dunning, T. H., Jr. Gaussian basis sets for use in correlated molecular calculations. I. The atoms boron through neon and hydrogen. *J. Chem. Phys*. **1989**, *90*, 1007–1023.

74 Kendall, R. A.; Dunning, T. H., Jr.; Harrison, R. J. Electron affinities of the first-row atoms revisited. Systematic basis sets and wave functions. *J. Chem. Phys*. **1992**, *96*, 6796–6806.

75 Woon, D. E.; Dunning, T. H., Jr. Gaussian basis sets for use in correlated molecular calculations. III. The atoms aluminum through argon. *J. Chem. Phys*. **1993**, *98*, 1358–1371.

76 de Jong, W. A.; Harrison, R. J.; Dixon, D. A. Parallel Douglas–Kroll energy and gradients in NWChem: Estimating scalar relativistic effects using Douglas–Kroll contracted basis sets. *J. Chem. Phys.* **2001**, *114*, 48–53.

77 Dunning, T. H. Jr.; Peterson, K. A. Wilson, A. K. Gaussian basis sets for use in correlated calculations. X. The atoms aluminum through argon revisited. *J. Chem. Phys.* **2001**, *114*, 9244–9253.

78 Peterson, K. A.; Dunning, T. H., Jr. Accurate correlation consistent basis sets for molecular core–valence correlation effects: The second row atoms Al–Ar, and the first row atoms B–Ne revisited. *J. Chem. Phys*. **2002**, *117*, 10548–10560.

79 Yockel, S.; Wilson, A. K. Core-valence correlation consistent basis sets for second-row atoms (Al–Ar) revisited. *Theor. Chem. Acc*. **2008**, *120*, 119–131.

80 Douglas, M.; Kroll, N. M. Quantum electrodynamical corrections to the fine structure of helium. *Ann. Phys. (N.Y.)* **1974**, *82*, 89–155.

81 Jansen, G.; Hess, B. A. Revision of the Douglas-Kroll transformation. *Phys. Rev. A* **1989**, *39*, 6016–6017.

82 Visscher, L.; Dyall, K. G. Dirac–Fock atomic electronic structure calculations using different nuclear charge distributions. *Atomic Data and Nuclear Data Tables*, 1997, 67, 207-224.)

83 Frisch, M. J., Trucks, G. W., Schlegel, H. B., Scuseria, G. E., Robb, M. A., Cheeseman, J. R., *et al*. Gaussian 09 (revision D.01), Gaussian, Inc., Wallingford CT, 2009.

84 Zhao, Y.; Peverati, R.; Yang, R. K.; Luo, S.; Yu, H.; He, X.; Truhlar, D. G. MN-GFM, version 6.7: Minnesota Gaussian Functional Module; University of Minnesota: Minneapolis, MN, 2016.

85 Perdew, J. P.; Ruzsinsky, A.; Csonka, G. I.; Vydrov, O. A.; Scuseria, G. E.; Constantin, L. A.; Zhou, X.; Burke, K. Restoring the density-gradient expansion for exchange in solids and surfaces. *Phys. Rev. Lett.* **2008,** *100*, 136406-1–136406-4.

86 Zhao, Y.; Truhlar, D. G. Construction of a generalized gradient approximation by restoring

the density-gradient expansion and enforcing a tight Lieb–Oxford bound. *J. Chem. Phys.* **2008**, *128*, 184109-1–184109-8.

87 Peverati, R.; Zhao, Y.; Truhlar, D. G. Generalized gradient approximation that recovers the second-order density-gradient expansion with optimized across-the-board performance. *J. Phys. Chem. Lett.* **2011**, *2*, 1991–1997.

88 Becke, A. D. Density-functional exchange-energy approximation with correct asymptotic behavior. *Phys. Rev. A* **1988**, *38*, 3098–3100.

89 Lee, C.; Yang, W.; Parr, R. G. Development of the Colle-Salvetti correlation-energy formula into a functional of the electron density. *Phys. Rev. B* **1988**, *37*, 785–789.

90 Schultz, N. E.; Zhao, Y.; Truhlar, D. G. Density functionals for inorganometallic and organometallic chemistry. *J. Phys. Chem. A* **2005**, *109*, 11127–11143.

91 Lee, C.; Yang, W.; Parr, R. G. Development of the Colle-Salvetti correlation-energy formula into a functional of the electron density. *Phys. Rev. B* **1988**, *37*, 785–789.

92 Handy, N. C.; Cohen, A. J. Left-right correlation energy. *Mol. Phys.* **2001**, *99*, 403–412.

93 Thakkar, A. J.; McCarthy, S. P. Toward improved density functionals for the correlation energy. *J. Chem. Phys.* **2009**, *131*, 134109-1–134109-12.

94 Perdew, J. P.; Burke, K.; Ernzerhof, M. Ernzerhof, M. Generalized gradient approximation made simple. *Phys. Rev. Lett.* **1996**, 77, 3865–3868.

95 Zhang, Y.; Yang, W. Comment on "Generalized Gradient Approximation Made Simple. *Phys. Rev. Lett.* **1998**, *80*, 890.

96 Hammer, B.; Hansen, L. B.; Norskov, J. K. Improved adsorption energetics within density-functional theory using revised Perdew-Burke-Ernzerhof functionals. *Phys. Rev. B* **1999**, *59*, 7413–7421.

97 Yu, H. S.; Zhang, W.; Verma, P.; He, X.; Truhlar, D. G. Nonseparable exchange–correlation functional for molecules, including homogeneous catalysis involving transition metals. *Phys. Chem. Chem. Phys.* **2015**, *17*, 12146–12160.

98 Peverati, R.; Truhlar, D. G. Exchange–correlation functional with good accuracy for both structural and energetic properties while depending only on the density and its gradient. *J. Chem. Theory Comput.* **2012**, *8*, 2310–2319.

99 Zhao, Y.; Truhlar, D. G. A new local density functional for main-group thermochemistry, transition metal bonding, thermochemical kinetics, and noncovalent interactions. *J. Chem. Phys.* **2006**, *125*, 194101-1–194101-18.

100 Wang, Y.; Jin, X.; Yu, H. S.; Truhlar, D. G.; He, X. Revised M06-L functional for improved accuracy on chemical reaction barrier heights, noncovalent interactions, and solid-state physics. *Proc. Natl. Acad. Sci. U.S.A.* **2017**, *114*, 8487–8492.

101 Peverati, R.; Truhlar, D. G. Improving the accuracy of hybrid meta-GGA density functionals by range separation. *J. Phys. Chem. Lett.* **2011**, *2*, 2810–2817.

102 Sun, J.; Haunschild, R.; Xiao, B.; Bulik, I. W.; Scuseria G. E.; Perdew, J. P. Semilocal and hybrid meta-generalized gradient approximations based on the understanding of the kinetic-energy-density dependence. *J. Chem. Phys.* **2013**, *138*, 044113-1–044113-8.

103 Boese, A. D.; Handy, N. C. New exchange-correlation density functionals: The role of the kinetic-energy density. *J. Chem. Phys.* **2002**, *116*, 9559–9569.

104 Peverati, R.; Truhlar, D. G. An improved and broadly accurate local approximation to the exchange–correlation density functional: The MN12-L functional for electronic structure calculations in chemistry and physics. *Phys. Chem. Chem. Phys.* **2012**, *14*, 13171–13174.

105 Yu, H. S.; He, X.; Truhlar, D. G. MN15-L: A New local exchange-correlation functional for

Kohn–Sham density functional theory with broad accuracy for atoms, molecules, and solids. *J. Chem. Theory Comput.* **2016**, *12*, 1280–1293.

106 Adamo, C.; Barone, V. Toward reliable adiabatic connection models free from adjustable parameters. *Chem. Phys. Lett.* **1997**, *274*, 242–250.

107 Stephens, P. J.; Devlin; Chabalowski, C. F.; Frisch, M. J. Ab initio calculation of vibrational absorption and circular dichroism spectra using density functional force fields. *J. Phys. Chem.* **1994**, *98*, 11623–11627.

108 Hamprecht, F. A.; Cohen, A.; Tozer, D. J.; Handy, N. C. Development and assessment of new exchange-correlation functionals. *J. Chem. Phys*. **1998**, *109*, 6264–6271.

109 Keal, T. W.; Tozer, D. J. Semiempirical hybrid functional with improved performance in an extensive chemical assessment. *J. Chem. Phys.* **2005**, *123*, 121103-1–121103-4.

110 Zhao, Y.; Truhlar, D. G. Hybrid meta density functional theory methods for thermochemistry, thermochemical kinetics, and noncovalent interactions: The MPW1B95 and MPWB1K models and comparative assessments for hydrogen bonding and van der Waals interactions. *J. Phys. Chem. A* **2004**, *108*, 6908–6918.

111 Lynch, B. J.; Fast, P. L.; Harris, M.; Truhlar, D. G. Adiabatic connection for kinetics. *J. Phys. Chem. A* **2000**, *104*, 4811–4815.

112 Zhao, Y.; Truhlar, D. G. Hybrid meta density functional theory methods for thermochemistry, thermochemical kinetics, and noncovalent interactions: The MPW1B95 and MPWB1K models and comparative assessments for hydrogen bonding and van der Waals interactions. *J. Phys. Chem. A* **2004**, *108*, 6908–6918.

113 Hoe, M. W.; Cohen, A. J.; Handy, N. C. Assessment of a new local exchange functional OPTX. *Chem. Phys. Lett.* **2001**, *341*, 319–328.

114 Adamo, C.; Barone, V. Toward reliable density functional methods without adjustable parameters: The PBE0 model. *J. Chem. Phys.* **1999**, *110*, 6158–6170.

115 Peverati, R.; Truhlar, D. G. Communication: A global hybrid generalized gradient approximation to the exchange-correlation functional that satisfies the second-order density-gradient constraint and has broad applicability in chemistry. *J. Chem. Phys.* **2011**, *135*, 191102-1–191102-4.

116 Krieger, J. B.; Chen, J.; Iafrate, G. J.; Savin, A. In *Electron Correlations and Materials Properties*; Gonis, A.; Kioussis, N., Eds.; Plenum: New York, **1999**, pp 463

117 Zhao, Y.; Truhlar, D. G. Density functionals with broad applicability in chemistry. *Acc. Chem. Res.* **2008**, *41*, 157–167.

118 Zhao, Y.; Truhlar, D. G. Exploring the limit of accuracy of the global hybrid meta density functional for main-group thermochemistry, kinetics, and noncovalent interactions. *J. Chem. Theory Comput.* **2008**, *4*, 1849–1868.

119 Zhao, Y.; Lynch, B. J.; Truhlar, D. G. Multi-coefficient extrapolated density functional theory for thermochemistry and thermochemical kinetics. *Phys. Chem. Chem. Phys.* **2005**, *7*, 43–52.

120 Zhao, Y.; Truhlar, D. G. The M06 suite of density functionals for main group thermochemistry, thermochemical kinetics, non- covalent interactions, excited states, and transition elements: two new functionals and systematic testing of four M06-class functionals and 12 other functionals. *Theor. Chem. Acc.* **2008**, *120*, 215–241.

121 Wang, Y.; Verma, P.; Jin, X.; Truhlar, D. G.; He, X. Revised M06 density functional for main-group and transition-metal chemistry. *Proc. Natl. Acad. Sci. U.S.A*. **2018**, *115*, 10257–10262.

122 Zhao, Y.; Truhlar, D. G. Density functional for spectroscopy: No long-range self-interaction

error, good performance for Rydberg and charge-transfer states, and better performance on average than B3LYP for ground states. *J. Phys. Chem. A* **2006**, *110*, 13126–13130.

123 Zhao, Y.; Truhlar, D. G. Design of density functionals that are broadly accurate for thermochemistry, thermochemical kinetics, and nonbonded interactions. *J. Phys. Chem. A* **2005**, *109*, 5656–5667.

124 Staroverov, V. N.; Scuseria, G. E.; Tao, J.; Perdew, J. P. Comparative assessment of a new nonempirical density functional: Molecules and hydrogen-bonded complexes. *J. Chem. Phys.* **2003**, *119*, 12129–12137.

125 Boese, A. D.; Handy, N. C. New exchange-correlation density functionals: The role of the kinetic-energy density. *J. Chem. Phys.* **2002**, *116*, 9559–9569.

126 Yu, H. S.; He, X.; Li, S. L.; Truhlar, D. G. MN15: A Kohn–Sham global-hybrid exchange–correlation density functional with broad accuracy for multi-reference and single-reference systems and noncovalent interactions. *Chem. Sci.* **2016**, 7, 5032–5051.

127 Heyd, J.; G. E. Scuseria, G. E.; Ernzerhof, M. Hybrid functionals based on a screened Coulomb potential. *J. Chem. Phys.* **2003**, *118*, 8207–8215.

128 Henderson, T. M.; Izmaylov, A. F.; Scalmani, S.; Scuseria, G. E. Can short-range hybrids describe long-range-dependent properties? *J. Chem. Phys.* **2009**, *131*, 044108-1–044108-9.

129 Chai, J.; Head-Gordon, M. Systematic optimization of long-range corrected hybrid density functionals. *J. Chem. Phys.* **2008**, *128*, 084106-1–084106-15.

130 Chai, J.; Head-Gordon, M. Long-range corrected hybrid density functionals with damped atom–atom dispersion corrections. *Phys. Chem. Chem. Phys.* **2008**, *10*, 6615–6620.

131 Peverati, R.; Truhlar, D. G. Improving the accuracy of hybrid meta-GGA density functionals by range separation. *J. Phys. Chem. Lett.* **2011**, *2*, 2810–2817.

132 Verma, P.; Wang, Y.; Ghosh, S.; He, X.; Truhlar, D. G. Revised M11 exchange-correlation functional for electronic excitation energies and ground-state properties. *J. Phys. Chem. A* **2019**, *123*, 2966–2990.

133 Peverati, R.; Truhlar, D. G. Screened-exchange density functionals with broad accuracy for chemistry and solid-state physics. *Phys. Chem. Chem. Phys.* **2012**, *14*, 16187–16191.

134 Lynch, B. J.; Truhlar, D. G. Multilevel methods for thermochemistry and thermochemical kinetics. *ACS Symp. Ser.* **2007***, 958*, 153–167.

135 Helgaker, T.; Klopper, W.; Tew, D. P. 2008, Quantitative quantum chemistry. *Mol. Phys.* **2008**, *106*, 2107-2143.

136 Raghavachari, K.; Saha, A. Accurate composite and fragment-based quantum chemical models for large molecules. *Chem. Rev.* **2015**, *115*, 5643-5677.

137 Peterson, C.; Penchoff, D. A.; Wilson, A. K. Prediction of thermochemical properties across the periodic table: A review of the correlation consistent composite approach (ccCA) strategies and applications. *Annu. Rep. Comput. Chem.* **2016***, 12*, 3-45.

138 Zhao, Y.; Xia, L.; He, Q.; Zhao, M. X.; Truhlar, D. G. Extrapolation of high-order correlation energies: the WMS model. *Phys. Chem. Chem. Phys.* **2018**, *20,* 27375–27384.

139 Zhang, W.; Kong, X.; Liu, S.; Zhao, Y. Multi-coefficients correlation methods. *Wiley Interdis. Rev. Comput. Mol. Sci.* **2020**, in press. doi:10.1002/wcms.1474

140 Karton, A.; Rabinovich, E.; Martin, J. M. L.; Ruscic, B. W4 theory for computational thermochemistry: In pursuit of confident sub-kJ/mol predictions. *J. Chem. Phys*. **2006**, *125*, 144108-1–144108-17.

141 Tajti, A.; Szalay, P. G.; Csaszar, A. G.; Kallay, M.; Gauss, J.; Valeev, E. F.; Flowers, B. A.; Vazquez, J.; Stanton, J. F. HEAT: High accuracy extrapolated ab initio thermochemistry. *J. Chem. Phys*. **2004**, *121*, 11599–11613.

142 Harding, M. E.; Vazquez, J.; Ruscic, B.; Wilson, A. K.; Gauss, J.; Stanton, J. F. High-accuracy extrapolated ab initio thermochemistry. III. Additional improvements and overview. *J. Chem. Phys.* **2008**, *128*, 114111-1–114111-15.

143 Thorpe, J. H.; Lopez, C. A.; Nguyen, T. L.; Baraban, J. H.; Bross, D. H.; Ruscic, B.; Stanton, J. F. High-accuracy extrapolated ab initio thermochemistry. IV. A modified recipe for computational efficiency. *J. Chem. Phys.* **2019**, *150*, 224102-1–224102-16.

144 Peterson, K. A.; Feller, D.; Dixon, D. A. Chemical accuracy in ab initio thermochemistry and spectroscopy: current strategies and future challenges. *Theo Chem Acc* **2012**, *131*, 1079.

145 Long, B., Bao, J. L., Truhlar, D. G. Kinetics of the strongly correlated $CH_3O + O_2$ reaction: The importance of quadruple excitations in atmospheric and combustion chemistry *J. Am. Chem. Soc*. **2019**, *141*, 611–617.

146 Kallay, M. Surjan, P. R. Higher excitations in coupled-cluster theory. *J. Chem. Phys.* **2005**, *115*, 2945–2954.

147 Helgaker, T.; Klopper, W.; Koch, H.; Noga, J. Basis-set convergence of correlated calculations on water. *J. Chem. Phys.* **1997**, *106*, 9639.

148 Bomble, Y. J.; Stanton, J. F.; Kallay, M.; Gauss, J. Coupled-cluster methods including noniterative corrections for quadruple excitations. *J. Chem. Phys.* **2005**, *123,* 054101-1–054101-8

149 Kallay, M. MRCC, A String-Based Quantum Chemical Program Suite; Budapest University of Technology and Economics: 2001

150 Herzberg, G. *Spectra of diatomic Molecule*s; 2nd ed.; Van Nostrand: Princeton, 1950.

151 Sansonetti, J.; Martin, W. Young, S. Handbook of Basic Atomic Spectroscopic Data; Version 1.00, National Institute of Standards and Technology: Gaithersburg, MD, 2003. Available at http://physics.nist. gov/Handbook (accessed Aug 10, 2016).

152 Werner, H.-J.; Knowles, P. J. A second order multiconfiguration SCF procedure with optimum convergence. *J. Chem. Phys*. **1985**, *82*, 5053–5063.

153 Knowles, P. J.; Werner, H.-J. An efficient second-order MC SCF method for long configuration expansions. *Chem. Phys. Lett*. **1985**, *115*, 259–267.

154 Langhoff, S. R. and Kern, C. W. **1977**, Modern Theoretical Chemistry, Vol.3 (New York: Plenum Press).

155 Bethe, H. A. and Salpeter, E. E. **1957**, Quantum Mechanics of One- and Two-Electron Atoms (Berlin: Springer-Verlag).

156 Zheng, J.; Xu, X.; Truhlar, D. G. Minimally augmented Karlsruhe basis sets. *Theor. Chem. Acc.* **2011**, *128*, 295–305.

157 Weigend, F.; Ahlrichs, R. Balanced basis sets of split valence, triple zeta valence and quadruple zeta valence quality for H to Rn: Design and assessment of accuracy. *Phys. Chem. Chem. Phys.* **2005***, 7*, 3297–3305.

158 Wernel,H.-J.;Knowles,P.J.;Knizia,G.;Manby,F.R.;Schütz,M.; Celani, P.; Korona, T.; Lindh, R.; Mitrushenkov, A.; Rauhut, G.; Shamasundar, K. R.; Adler, T. B.; Amos, R. D.; Bernhardsson, A.; Berning, A.; Cooper, D. L.; Deegan, M. J. O.; Dobbyn, A. J.; Eckert, F.; Goll,E.; Hampel,C.; Hesselmann,A.; Hetzer,G.; Hrenar,T.; Jansen,G.; Köppl, C.; Liu, Y.; Lloyd, A. W.; Mata, R. A.; May, A. J.; McNicholas, S. J.; Meyer, W.; Mura, M. E.; Nicklass, A.; O'Neill, D. P.; Palmieri, P.; Pflüger, K.; Pitzer, R.; Reiher, M.; Shiozaki, T.; Stoll, H.; Stone, A. J.; Tarroni, R.; Thorsteinsson, T.; Wang, M.; Wolf, A. Molpro, version 2015.1, A Package of Ab Initio Programs; available via the Internet at: http://www.molpro.net.

159 Seeger, R.; Pople, J. A. Self-consistent molecular orbital methods. XVIII. Constraints and stability in Hartree– Fock theory. *J. Chem. Phys*. **1977**, *66*, 3045–3050.

160 Bauernschmitt, R.; Ahlrichs, R. Stability analysis for solutions of the closed shell Kohn–Sham equation. *J. Chem. Phys*. **1996**, *104*, 9047–9052.

161 Bao, J. L., Zhang, X., Truhlar, D. G. Predicting bond dissociation energy and bond length for bimetallic diatomic molecules: A challenge for electronic structure theory. *Phys. Chem. Chem. Phys*. **2017**, *19*, 5839–5854.

162 Pekeris, C. L. The rotation-vibration coupling in diatomic molecules. *Phys. Rev*. **1933**, *45*, 98–103.

163 Alecu, I. M.; Zheng, J.; Zhao, Y.; Truhlar, D. G. Computational thermochemistry: Scale factor databases and scale factors for vibrational frequencies obtained from electronic model chemistries. *J. Chem. Theory Comput*. **2010**, *6*, 2872–2887.

164 Levine I. N. **1975**, *Molecular Spectroscopy* (John Wiley & Sons, Inc., New York).

165 Lee, T. J.; Taylor, P. R. A diagnostic for determining the quality of single-reference electron correlation methods. *Int. J. Quantum Chem. Symp*. **1989**, *23*, 199–207.

166 Fogueri, U. R.; Kozuch, S.; Karton, A.; Martin, J. M. L. A simple DFT-based diagnostic for nondynamical correlation. *Theor. Chem. Acc.* **2013**, *132*, 1291.

167 Janssen, C. L.; Nielsen, I. M. B. New diagnostics for coupled-cluster and Møller-Plesset perturbation theory. *Chem. Phys. Letters*. **1998**, *290*, 423-430.

168 Jiang, W.; Manivasagam, S.; Wilson, A.K. Multireference character for 4d transition metal-containing molecules. *J. Chem. Theory Comput*. **2015**, *11*, 5865–5872.

169 Jiang, W.; DeYonker, N. J.; Wilson, A. K. Multireference character for 3d transition-metal-containing molecules. *J. Chem. Theory Comput*. **2012**, *8*, 460–468.

170 Tishchenko, O.; Zheng, J.; Truhlar, D. G. Multireference model chemistries for thermochemical kinetics. *J. Chem. Theory Comput*. **2008**, *4*, 1208-1219.

171 Bao, J. L.; Gagliardi, L.; Truhlar, D. G. Self-interaction error in density functional theory: An appraisal. *J. Phys. Chem. Lett*. **2018**, *9*, 2353–2358.